Episodic Trade Wind Regimes over the Western Pacific Warm Pool

RICHARD H. JOHNSON AND XIN LIN

Department of Atmospheric Science, Colorado State University, Fort Collins, Colorado

(Manuscript received 1 August 1996, in final form 26 February 1997)

ABSTRACT

The western Pacific warm pool experiences the greatest rainfall of any oceanic region on earth. While the SST is everywhere high over the warm pool, there is great spatial and temporal variability in rainfall. Sounding data from the recent TOGA COARE are used to document this variability. In particular, the vertical distributions of heating and moistening at different phases of the 30–60 day or intraseasonal oscillation are determined for different areas within the warm pool.

While heating and moistening distributions near the equator over the warm pool are often similar to those observed over the western Pacific within the convectively active ITCZ, these profiles do not prevail at all times. In particular, during westerly wind bursts and suppressed, light-wind periods, heating and moistening distributions over the COARE Intensive Flux Array frequently resemble those observed in the trade wind belts. Such profiles are characterized by relatively large negative values of apparent moisture sink Q_2 in the lowest 2–3 km, reflecting the important moistening effects of shallow, mostly nonprecipitating cumulus clouds. A maximum in moistening commonly occurs in the lower part of the cloud layer during the westerly wind bursts, indicating many ''forced'' cumuli that are extensions of boundary-layer turbulence. During suppressed, light-wind periods the moistening peak shifts to the upper part of the cloud layer, indicating a larger proportion of ''active'' trade cumulus at that time (consistent with higher SSTs and weaker vertical wind shear).

A spectral cloud diagnostic model is used to determine the properties of the shallow cloud fields. Computed profiles of mass fluxes, entrainment, detrainment, and heat and moisture balances during these periods generally resemble those for the western Atlantic trade wind regime. These findings lead to the conclusion that, in association with the intraseasonal oscillation, the western Pacific warm pool boundary layer periodically develops trade-wind-like characteristics with abundant shallow cumulus, and these episodic ''tradelike'' regimes are frequent enough to impact the seasonal-mean distributions of boundary layer heating and moistening.

1. Introduction

The western Pacific warm pool coincides with the maximum in the global distribution of vertically integrated diabatic heating in the troposphere (e.g., Wei et al. 1983; Masuda 1984). Unlike the distribution of SST, however, which exhibits a broad, seasonally shifting maximum across the equator in the western Pacific [with a slight cool tongue along the equator near the date line; e.g., Reynolds and Smith (1995)] the distribution of rainfall is much more variable in time and space (e.g., Taylor 1973; Legates and Wilmott 1990; Spencer 1993). Annual mean rainfall distributions typically show an east–west ITCZ band near 5°N across the Pacific and a band extending southeastward from the warm pool into the Southern Hemisphere along the South Pacific convergence zone (SPCZ) (e.g., Kiladis et al. 1989). In addition, there is pronounced temporal variability of convection in the western Pacific, ranging all the way from interannual, annual, and seasonal timescales to the 30–60 day timescale of the intraseasonal oscillation (Madden and Julian 1971) with their associated westerly wind bursts (e.g., Kiladis et al. 1994), down to 2-day waves and diurnally modulated convection (e.g., Nakazawa 1988; Chen et al. 1996).

Determination of this wide-ranging temporal and spatial variability of convection over the warm pool was one of the principal objectives of the recent Tropical Ocean Global Atmosphere Coupled Ocean–Atmosphere Response Experiment (TOGA COARE; Webster and Lukas 1992). Of interest for this study is the vertical and horizontal distribution of heating and moistening over the warm pool. This subject is important in several regards. First, it has been shown by Luo and Yanai (1984) and others that the differences in the vertical profiles of heating and moistening yield important information about the nature of the precipitation systems, for example, the relative contributions of convective and stratiform rainfall. Also, modeling studies of the Walker circulation (Hartmann et al. 1984) and the intraseasonal oscillation (Sui and Lau 1989) have detected an important sensitivity in their models to the location of the height of peak heating. However, additionally, as will

Corresponding author address: Richard H. Johnson, Department of Atmospheric Science, Colorado State University, Fort Collins, CO 80523.
E-mail: rhj@vortex.atmos.colostate.edu

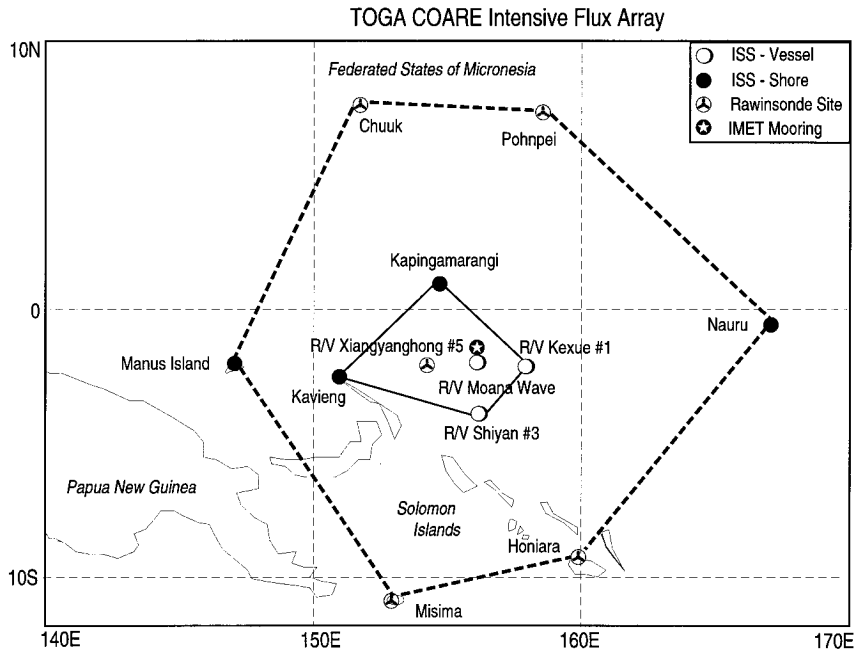

FIG. 1. Sounding stations within the TOGA COARE Outer Sounding Array (outer polygon) and Intensive Flux Array (inner polygon).

be seen in this study, these distributions shed insight into the nature of cloud populations and boundary-layer processes over the warm pool.

In a recent paper, Lin and Johnson (1996b) computed the ''apparent heat source'' Q_1 and ''apparent moisture sink'' Q_2 (Yanai et al. 1973) within the COARE domain. The seasonal, or four-month mean, vertical distributions of Q_1 and Q_2 were found to vary significantly across the domain. In the heavily raining ITCZ and SPCZ, the Q_1 and Q_2 profiles resemble those determined for the western Pacific Marshall Islands region by Reed and Recker (1971), Nitta (1972), and Yanai et al. (1973), namely, positive values throughout the troposphere with the Q_1 maximum displaced above the Q_2 maximum, characteristic of vigorous deep convective activity. However, the seasonal-mean profile of Q_2 centered near the equator within the COARE IFA (Intensive Flux Array) is considerably different from the ITCZ region. Specifically, negative values of Q_2 (indicating moistening) were observed from the surface to 1.5 or 2 km. Since the most prominent occurrences of negative Q_2 were during westerly wind bursts, Lin and Johnson (1996b) speculated that the low-level moistening may be a consequence of vigorous boundary-layer mixing and shallow nonprecipitating cumulus clouds during these high-wind periods, similar to that found in the trade wind belt of the Atlantic (e.g., Nitta and Esbensen 1974; Nitta 1975). Such nonprecipitating clouds, which are known to be a prominent fixture of much of the tropical western Pacific (e.g., Riehl et al. 1951; Malkus 1954; Malkus and Riehl 1964) were reported by Williams et al. (1996) to have been ''prolific'' over the warm pool during COARE. In this paper, this subject is explored further by examining heat and moisture budgets in greater detail. We find that the tradelike cumulus regimes are not only prominent during the westerly wind bursts but also during suppressed, light-wind periods. Finally, a diagnostic cloud model is used to infer properties of the cloud fields.

2. Data analysis and procedures

Heat and moisture budgets have been computed for the COARE Outer Sounding Array (OSA) and Intensive Flux-Array (Fig. 1) using 6-hourly sounding data for the 4-month Intensive Observing Period (IOP; 1 November 1992–28 February 1993). Quality control procedures and other details of the sounding dataset can be found in Lin and Johnson (1996a). However, in addition to those procedures the raw sounding data from sites with Integrated Sounding Systems (ISSs; Parsons et al. 1994) have been augmented by 915-MHz wind profiler data to fill in for gaps in the ISS Omegasonde low-level winds that arose due to signal problems. The procedure to merge the Omegasonde and profiler winds is described in Ciesielski et al. (1997). Since our study focuses principally on low-level features, this merging process is considered essential for obtaining reliable diagnoses of the properties of the shallow cloud fields.

In the application of the cloud spectral diagnostic model, the vertical profile of net radiative heating Q_R is required. Observed profiles for the full range of atmospheric conditions are not available. In this study, the primary emphasis will be on periods with shallow

cumulus clouds, although some occasional cirrus and other clouds coexisted with the shallow cumulus. While it is an oversimplification for the problem at hand, we have used the National Center for Atmospheric Research Community Climate Model (CCM2) one-dimensional radiation code (Kiehl et al. 1994) to compute the shortwave and longwave radiative heating profiles at 6-hourly intervals based on IFA sounding, surface, and SST data. Effects of cloud layers are excluded from the algorithm we have used, so there are obvious limitations to this procedure. Nevertheless, the deduced profiles for the days with scattered shallow cumulus and few clouds aloft (characteristic of many of the days) are expected to be somewhat reasonable.

3. Observed heating and moistening distributions

The apparent heat source Q_1 and the apparent moisture sink Q_2 are computed from the defining expressions:

$$Q_1 \equiv c_p\left[\frac{\partial \bar{T}}{\partial t} + \bar{\mathbf{v}}\cdot\nabla\bar{T} + \left(\frac{p}{p_0}\right)^{\kappa}\bar{\omega}\frac{\partial\bar{\theta}}{\partial p}\right]$$

$$= Q_R + L(\bar{c} - \bar{e}) - c_p\left(\frac{p}{p_0}\right)^{\kappa}\frac{\partial\overline{\omega'\theta'}}{\partial p}, \qquad (1)$$

$$Q_2 \equiv -L\left[\frac{\partial\bar{q}}{\partial t} + \bar{\mathbf{v}}\cdot\nabla\bar{q} + \bar{\omega}\frac{\partial\bar{q}}{\partial p}\right]$$

$$= L(\bar{c} - \bar{e}) + L\frac{\partial\overline{\omega'q'}}{\partial p}, \qquad (2)$$

where T is temperature, θ potential temperature, q mixing ratio of water vapor; c condensation rate, e evaporation rate; $\kappa = R/c_p$ for R and c_p gas constant and the specific heat at constant pressure of dry air respectively, L latent heat of condensation, $p_0 = 1000$ mb, overbar refers to a horizontal average, and the horizontal eddy-flux divergences have been neglected.

The IOP-mean Q_1 and Q_2 profiles (normalized by precipitation rate following Johnson 1984) for the OSA and IFA are shown in Fig. 2. Values for the Marshall Islands region from Yanai et al. (1973) are shown for comparison. The OSA Q_1 and Q_2 profiles resemble those for the Marshall Islands, except for the smaller amplitude of Q_2. This difference can be explained by noting that the areas under the Q_2 curves are proportional to $1 - E_0/P_0$ (E_0: evaporation rate,[1] P_0: precipitation rate; Johnson 1984), which has the values 0.79 and 0.56 for the Marshall Islands and COARE OSA, respectively. In addition, both the COARE OSA and Marshall Islands Q_2 profiles show a minimum near 600 hPa or 4 km, which is associated with an inflection point in the specific humidity profile likely related in some way to the effects of melting (Johnson et al. 1996).

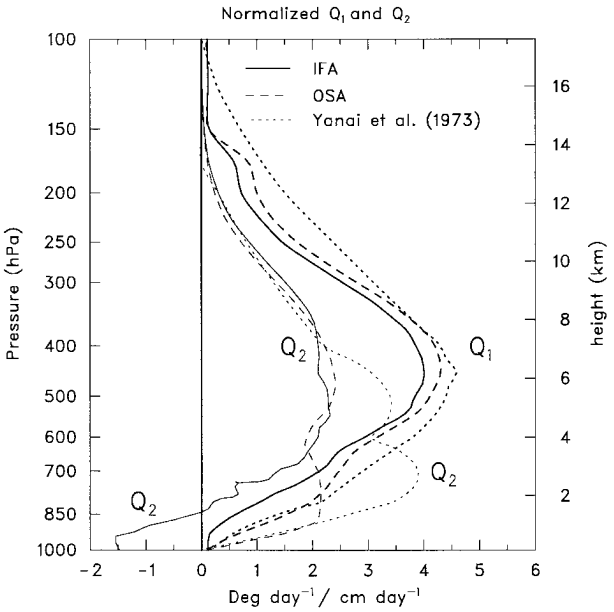

FIG. 2. Profiles of Q_1 (heavy lines) and Q_2 (light lines) normalized by precipitation rate for Intensive Flux Array (IFA, solid lines), Outer Sounding Array (OSA, long dashed lines) (both IOP means), and Marshall Islands (from Yanai et al. 1973, short dashed lines).

The Q_2 profile for the IFA, however, contrasts in several ways from those for the OSA and Marshall Islands. First, negative values can be seen below 850 hPa or 1.5 km. Second, the IFA Q_2 profile does not exhibit a prominent double-peak structure, at least for the IOP mean. There are times, however, when the IFA Q_2 profiles do resemble those for the ITCZ and Marshall Islands. An example is during a period of heavy rainfall on 11–17 December (Fig. 3), just prior to the strong westerly wind burst at the end of December (Gutzler et al. 1994; Kiladis et al. 1994). Averaged over this one-week period, Q_1 and Q_2 are positive everywhere and the peaks are displaced, indicative of deep convective activity (e.g., Yanai et al. 1973). A double peak in Q_2 is also present (though not very pronounced). Note from Fig. 3 that both Q_1 and Q_2 are considerably larger than Q_R (computed here only for general reference, assuming clear-sky conditions) during this convectively active period.

What, then, is the cause of the negative, IOP-averaged Q_2 at low levels within the IFA? To understand this behavior, we examine time series of Q_2 (five-day running means) for the entire IOP. For the larger area, the OSA, Q_2 is mostly positive throughout the troposphere, except for several short periods in November and early December (Fig. 4). Since from (2),

$$\frac{1}{g}\int_{p_T}^{p_s} Q_2\, dp = L(P_0 - E_0), \qquad (3)$$

where p_T is the tropopause pressure and p_s is the surface pressure (Yanai et al. 1973), mostly positive Q_2 implies

[1] E_0 has been computed by applying the bulk flux algorithm of Fairall et al. (1996) to mooring data within the IFA using a procedure described in Lin and Johnson (1996b).

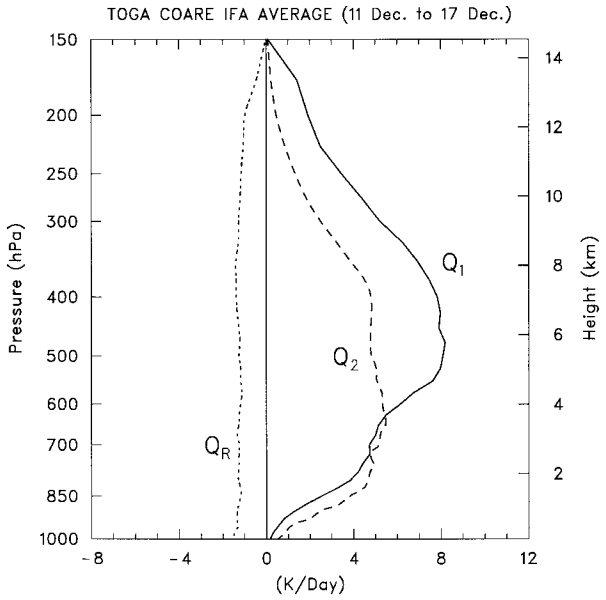

FIG. 3. IFA-averaged Q_1, Q_2, and Q_R profiles for convectively disturbed period (11–17 December 1992).

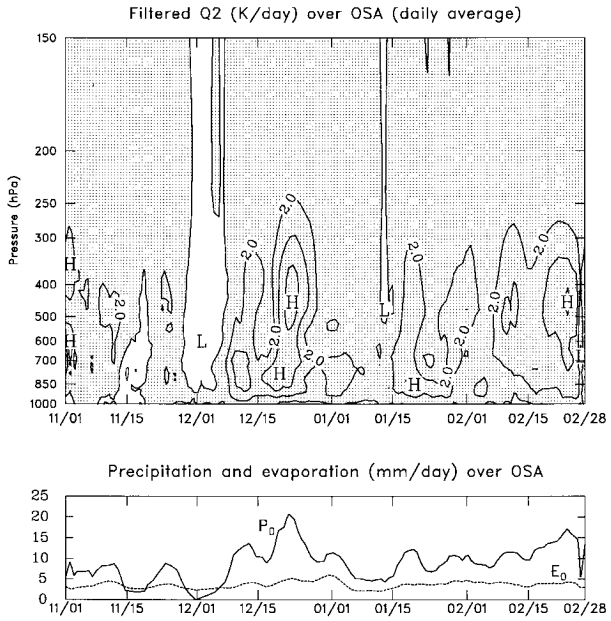

FIG. 4. IOP time series (five-day running means) of Q_2 (top panel, positive values shaded) and budget-derived precipitation rate P_0 and evaporation rate E_0 (bottom panel) for the Outer Sounding Array.

that P_0 exceeds E_0 most of the time. Indeed, this is true, except for brief periods in November and early December (bottom panel, Fig. 4). These results are not surprising considering that the area of the OSA is large enough to encompass significant precipitating systems for most of the IOP. In particular, the rainfall in this domain is heavy enough to produce a net positive Q_2 (net removal of water vapor) most of the time, implying a net transport of water vapor into the OSA ($P_0 > E_0$) on most days during the IOP.

In contrast, the time series of Q_2 for the much smaller IFA shows frequent periods of negative values (moistening), particularly in the lower troposphere (Fig. 5). Note, for example, the strong moistening below 800 hPa during the last two weeks of December and the first two weeks of February. These periods correspond to the two primary westerly wind bursts during COARE, as can be seen from the time series of the near-surface wind speed in the lower panel. It is also evident from the lower panel that E_0 is either approximately equal to or exceeds P_0 during significant portions of these strong-wind periods. This behavior is consistent with the apparent moistening (negative Q_2) in the lowest 2–3 km in Fig. 5. As will be seen, this apparent moistening is accomplished by mixed-layer turbulent transport as well as transport by shallow cumulus clouds (e.g., as in the Pacific and Atlantic trade wind belts; see Riehl et al. 1951; Augstein et al. 1973; Nitta and Esbensen 1974; Esbensen 1975; Brümmer 1978).

Also evident in Fig. 5 is a period of low-level moistening from mid November to early December. During this time, there was little precipitation and light winds (lower panel), except for brief disturbed periods on 24 and 27 November. Note that the maximum moistening (negative Q_2) peaked at a higher level (near 700 hPa) during the light-wind period than during the westerly burst periods.

Whether or not apparent moistening (negative Q_2) leads to an *actual* moistening depends on the balance of competing effects, namely, subsidence (which in the mixed layer is associated with dry-air entrainment) and advection. For example, the time series of 1000–700

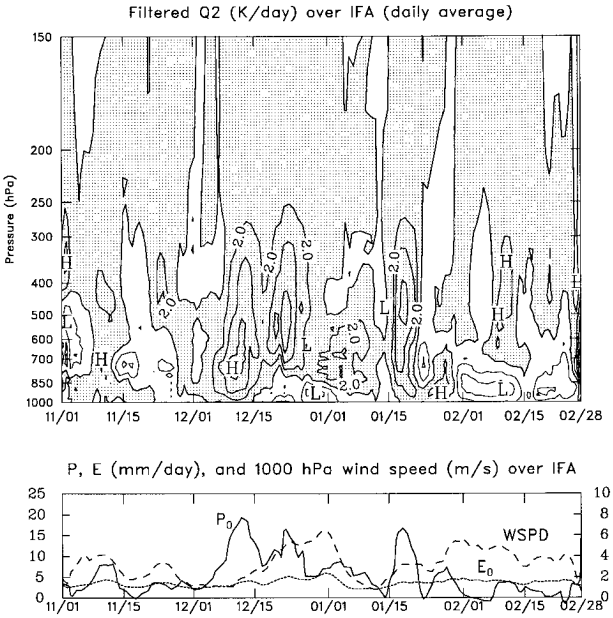

FIG. 5. As in Fig. 4 except for the Intensive Flux Array. Also, 1000-hPa wind speed has been added to the bottom panel.

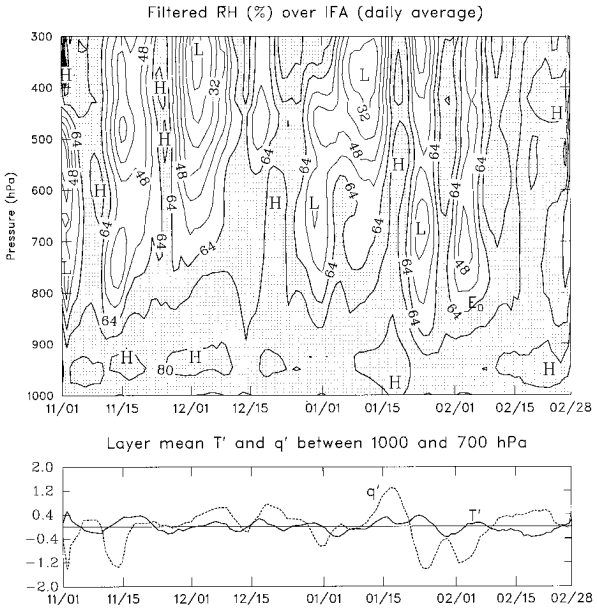

FIG. 6. Upper panel: Time series of daily mean relative humidity RH (%) (five-day running mean) over the Intensive Flux Array. Shaded area indicates RH $>$ 64%. Lower panel: Time series of IFA-averaged temperature and specific humidity deviations from the IOP mean (T' and q', K and g kg^{-1}).

hPa layer-averaged, IFA specific humidity deviation from the IOP-mean q' in Fig. 6 (lower panel) indicates prominent dry anomalies (negative q') during portions of the late December–early January and February westerly wind bursts, seemingly at odds with the negative Q_2 (moistenting) during this period. Noting that the temperature deviations T' are small (lower panel, Fig. 6), it can be seen from the time series of IFA relative humidity (upper panel) that these low-level dry excursions are principally associated with sharp midtropospheric dry anomalies. Such anomalies have been referred to as dry intrusions into the Tropics from the subtropics or ''dry tongues'' (Numaguti et al. 1995; Yoneyama and Fujitani 1995; Mapes and Zuidema 1996), apparently associated with perturbations in the meridional wind that accompany mixed Rossby–gravity waves (Numaguti et al. 1995). However, during the latter part of both westerly wind burst periods, the magnitudes of these negative q' values decrease, consistent with the apparent moistening (negative Q_2) at these times.

The mean profiles of Q_1 and Q_2 for the two westerly wind burst periods (27 December–3 January and 2–10 February; portions of the westerly wind burst periods when ships *Kexue 1* and *Shiyan 3* were on station) and the suppressed, light-wind period (15 November–5 December) are presented in Fig. 7. The averages shown are only for those times during these periods when $P_0 < 3.5$ mm day^{-1} (roughly the average evaporation rate during the IOP) in an attempt to isolate periods with predominantly nonprecipitating cumulus.[2] For this criterion, the averages in Fig. 7 represent 34%, 67%, and 50% of the total 6-hourly soundings for the December–January, February, and November–December cases, respectively. The patterns of Q_1 and Q_2 are similar for all periods: positive Q_1 near the surface with negative values above and negative Q_2 below 500 to 700 hPa. Above 700 hPa Q_1 and Q_2 are both generally small, except in the December–January case near 300–400 hPa. These upper-level positive values reflect the abundance of high clouds present during portions of this westerly wind burst (Velden and Young 1994). The low-level profiles are qualitatively similar to those determined by Nitta and Esbensen (1974) for undisturbed trade wind conditions during the Barbados Oceanographic and Meteorological Experiment (BOMEX) (Fig. 8), except that the levels of the maxima and minima differ from case to case.

Integrated budgets for the subcloud and cloud layers (following Betts 1975) for the above three periods are shown in Tables 1, 2, and 3. Three layers are defined: *subcloud layer*, surface to 950 hPa; *lower cloud layer*, 950–850 hPa (850 hPa is the approximate level of the saturation moist static energy h^* minimum); and *upper cloud layer*, 850–700 hpa. Here $\int (Q_1 - Q_R)\, dp$ represents the convective heating and $\int Q_2\, dp$ the convective moistening. In the subcloud layer there is an approximate balance between the vertical eddy heat flux convergence and radiative cooling ($\overline{c}$ is zero and $\overline{e}$ is small) during all three periods, as expected for trade wind mixed layers (Pennell and LeMone 1974; Betts 1975; LeMone and Pennell 1976; Nicholls and LeMone 1980). Also, in the subcloud layer there is moistening during all three periods, but it is greatest during the westerly wind bursts as a result of increased evaporation.

In the cloud layer, the profiles of $Q_1 - Q_R$ in the Atlantic trades (Fig. 8) and during the February westerly burst (Fig. 7b) are characterized by a cooling aloft and a warming below. This profile is also evident in the integrated heat budget (Table 2) with heating in the lower part of the cloud layer and cooling in the upper part (as in Betts 1975). Although the vertical divergence of the eddy heat flux in the cloud layer is not small (Nitta and So 1980), this $Q_1 - Q_R$ profile can in part be explained by an excess of evaporation over condensation in the upper half of the cloud layer and the reverse below. As illustrated in Fig. 8 and confirmed in the diagnostic study of Nitta (1975), this behavior occurs as cloud droplets, condensed in the lower part of the cloud layer, are carried aloft where they are detrained and evaporated (also see Betts 1975). The pronounced

[2] It should be noted, however, that some shallow cumulus which extended to only 2–3 km over the warm pool produced some precipitation (Rickenbach 1996), presumably as a result of the efficient collision–coalescence process over the exceptionally warm ocean surface.

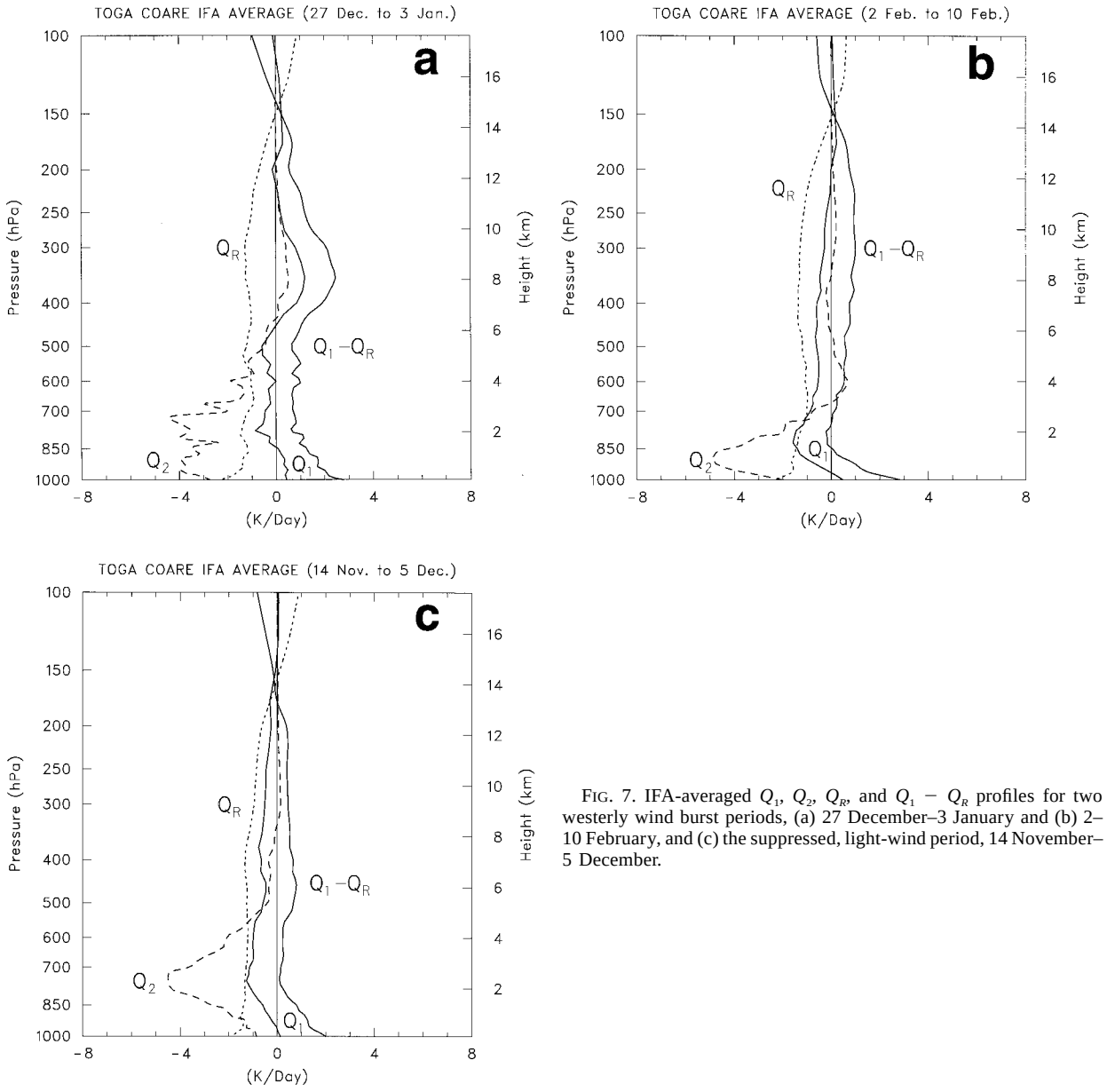

FIG. 7. IFA-averaged Q_1, Q_2, Q_R, and $Q_1 - Q_R$ profiles for two westerly wind burst periods, (a) 27 December–3 January and (b) 2–10 February, and (c) the suppressed, light-wind period, 14 November–5 December.

moistening in the upper part of the cloud layer is consistent with this explanation. That $Q_1 - Q_R$ in the December–January westerly wind burst and light-wind cases (Figs. 7a,c and Tables 1 and 3) is not quite negative in the upper part of the cloud layer may be an indication of precipitation occurring from some of the warm pool cumuli (despite their shallow depths) or from some deeper clouds in the region. The cloud and subcloud layers are closely coupled because it is the surface evaporation that provides the source for the moistening of the entire layer. For the steady-state tradewind boundary layer, the convective moistening by evaporation and eddy transports is offset by subsidence drying.

These findings suggest that the equatorial western Pacific behaves like the trade wind regime during the convectively suppressed (both strong and light wind) portions of the intraseasonal oscillation. During the light-wind period (14 November–5 December), both moistening and cooling peaks are located in the upper part of the cloud layer (Table 3) and at the same level (near 750 hPa, Fig. 7c), about 50 hPa higher than for the trade wind conditions in BOMEX (Fig. 8). This difference may be due to more active shallow cumuli and a weaker (and slightly deeper) trade wind inversion above a warmer sea surface in the western Pacific than in the Atlantic (Johnson et al. 1996). The Atlantic trade wind cooling and moistening peaks (Fig. 8) are much sharper than those over the warm pool (Fig. 7), presumably due

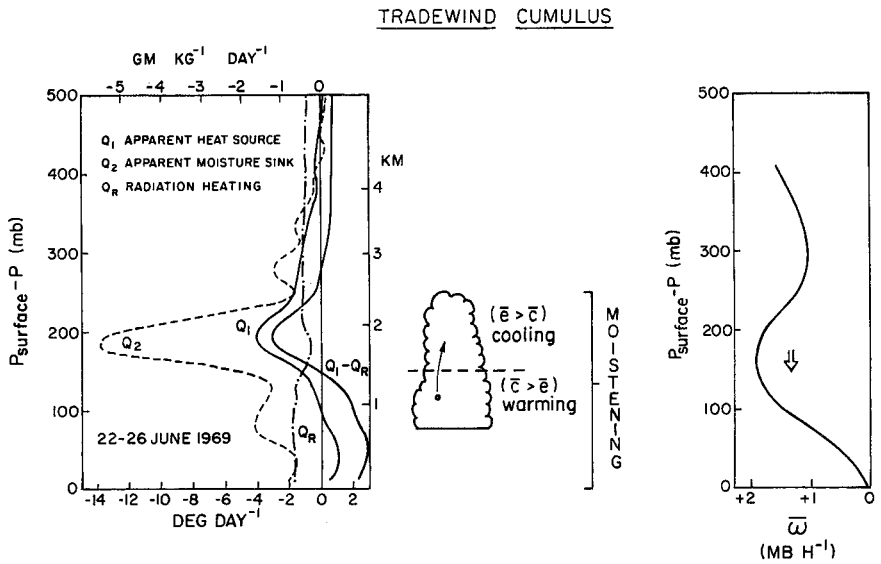

FIG. 8. Left: The observed Q_1, Q_2, Q_R, and $Q_1 - Q_R$ for the undisturbed BOMEX period 22–26 June 1969 (from Nitta and Esbensen 1974). Center: Schematic of trade wind cumulus layer showing effects of condensation $\bar{c}$ and evaporation $\bar{e}$ on the heat and moisture budgets. Right: Mean vertical p-velocity $\bar{\omega}$ over budget area.

to the sharper trade inversion which enhances evaporation near the top of the cumulus layer.

During the two westerly wind burst periods, significant moistening in the lower part of the cloud layer (Figs. 7a,b and Tables 1 and 2) is an indication of the prevalence of shallower cumulus clouds than the light-wind period. These contrasting cumulus regimes may be indicative of the two populations of tropical cumuli proposed by Esbensen (1978). One type, referred to as ''subinversion'' cumulus by Esbensen or ''forced'' cumulus by Stull (1985), are dynamically inactive clouds that are principally a reflection of overshooting of mixed-layer eddies. These may be the prevalent type of clouds during the high-wind periods (photographs of these cloud types will be shown later). Another type, ''inversion-penetrating'' cumulus (Esbensen 1978) or ''active'' cumulus (Stull 1985), experience considerable buoyancy and growth due to latent heat release. This type may predominate during the light-wind periods.

4. Diagnostic model results

In order to assess the specific roles of shallow-cumulus processes during the westerly wind burst periods, the spectral diagnostic method developed by Ogura and Cho (1973) and Nitta (1975) is used, which is based on the theory of cumulus parameterization proposed by Arakawa and Schubert (1974). This method has already been applied to shallow cumulus regimes in the eastern Atlantic (Nitta 1975) and East China Sea (Nitta and So 1980). The cloud model is an entraining plume updraft with detrainment in a thin layer at cloud top. Within this framework, detrainment over a deep layer is accomplished by cloud-top detrainment from a spectrum of cloud sizes. However, observational studies suggest that properties of shallow clouds are more complicated than this, characterized by updrafts and downdrafts and mixing between them (e.g., Malkus 1955; Betts and Albrecht 1987); asymmetric growth and detrainment patterns due to wind shear (Telford and Wagner 1980, Perry and Hobbs 1996), and cloud-top as well as lateral entrainment (e.g., Squires 1958). Recently, Barnes et al. (1996) found that the life cycle of shallow cumulus is characterized by a growth stage dominated by net entrainment, followed by a decay stage dominated by net detrainment. Since treatment of these effects within diagnostic models is difficult and we wish to compare our results with those of Nitta (1975) and Nitta and So

TABLE 1. Integrals of Q_R, $Q_1 - Q_R$, and Q_R (W m^{-2}) for subcloud layer, lower cloud layer, and upper cloud layer during the December–January westerly wind burst (27 December–3 January).

	$\int Q_R\,dp$	$\int (Q_1 - Q_R)dp$	$\int Q_2\,dp$
Upper cloud layer	−23.4	15.8	−62.3
Lower cloud layer	−15.7	19.1	−43.2
Subcloud layer	−10.9	13.3	−19.6

TABLE 2. Integrals of Q_R, $Q_1 - Q_R$, and Q_2 (W m^{-2}) for subcloud layer, lower cloud layer, and upper cloud layer during the February westerly wind burst (2–10 February).

	$\int Q_R\,dp$	$\int (XQ_1 - Q_R)dp$	$\int Q_2\,dp$
Upper cloud layer	−22.2	−1.2	−40.8
Lower cloud layer	−18.6	7.7	−55.0
Subcloud layer	−11.1	12.0	−18.1

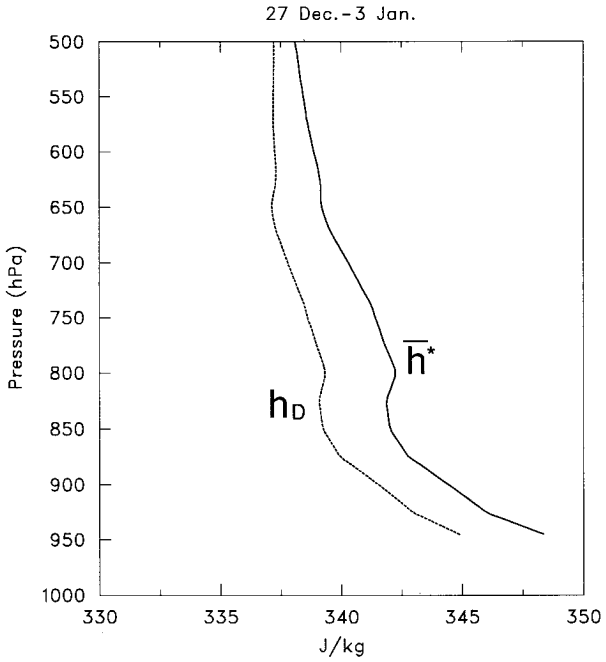

FIG. 9. Vertical profiles of saturation moist static energy of the environment h^* and moist static energy of the clouds at the detrainment level h_D during 27 December–3 January westerly wind burst.

TABLE 3. Integrals of Q_R, $Q_1 - Q_R$, and Q_2 (W m^{-2}) for subcloud layer, lower cloud layer, and upper cloud layer during a light-wind suppressed period (14 November–5 December).

	$\int Q_R\, dp$	$\int (Q_1 - Q_R)dp$	$\int Q_2\, dp$
Upper cloud layer	−23.6	5.2	−70.4
Lower cloud layer	−17.1	13.1	−21.6
Subcloud layer	−9.6	9.6	−5.8

(1980), we retain the Arakawa and Schubert (1974) cloud model framework.

The total mass flux in the clouds M_c is expressed by

$$M_c(p) = \int_0^{\lambda_D(p)} m_B(\lambda)\eta(p, \lambda)\, d\lambda, \tag{4}$$

where $m_B(\lambda)d\lambda$ is the subensemble mass flux, at the cloud base pressure p_B, due to the clouds whose fractional rates of entrainment are between λ and $\lambda + d\lambda$; $\eta(p, \lambda)$ is the normalized mass flux; and $\lambda_D(p)$ is the λ of clouds that detrain at pressure p. The mass detrainment $\delta(p)dp$ in the layer between p and $p + dp$ is equal to the subensemble mass flux due to clouds, which have parameter λ between $\lambda_D(p)$ and $\lambda_D(p) + (d\lambda_D(p)/dp)dp$, so that we can relate δ to m_B by

$$\delta(p) = m_B[\lambda_D(p)]\eta[p, \lambda_D(p)]\frac{d\lambda_D(p)}{dp}. \tag{5}$$

FIG. 10. A photograph taken from the R/V *Vickers* (2.1°S, 156.3°E) around 0100 UTC 26 December 1992 (courtesy of T. Rickenbach). The photograph shows shallow cumulus with tops near 2–2.5 km (assuming a cloud base of ~0.5 km) and higher clouds above. Photograph is one day prior to westerly burst period studied, so may not accurately portray conditions throughout it.

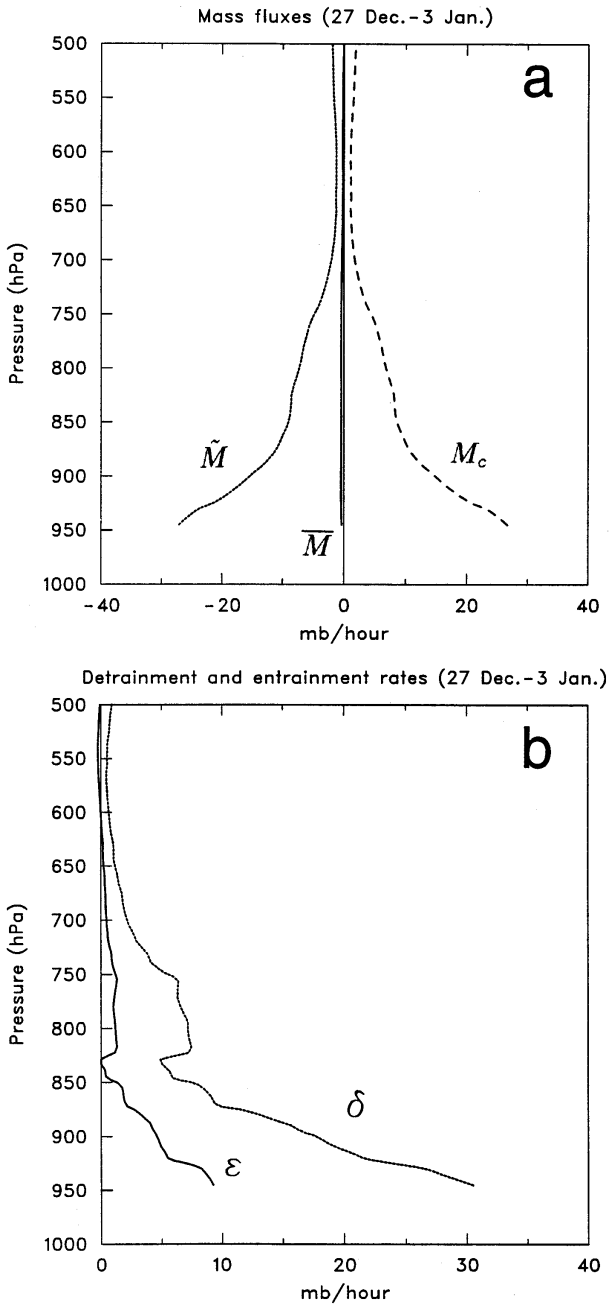

FIG. 11. (a) Mean, environmental, and cumulus mass fluxes and (b) entrainment and detrainment for the 27 December–3 January westerly wind burst.

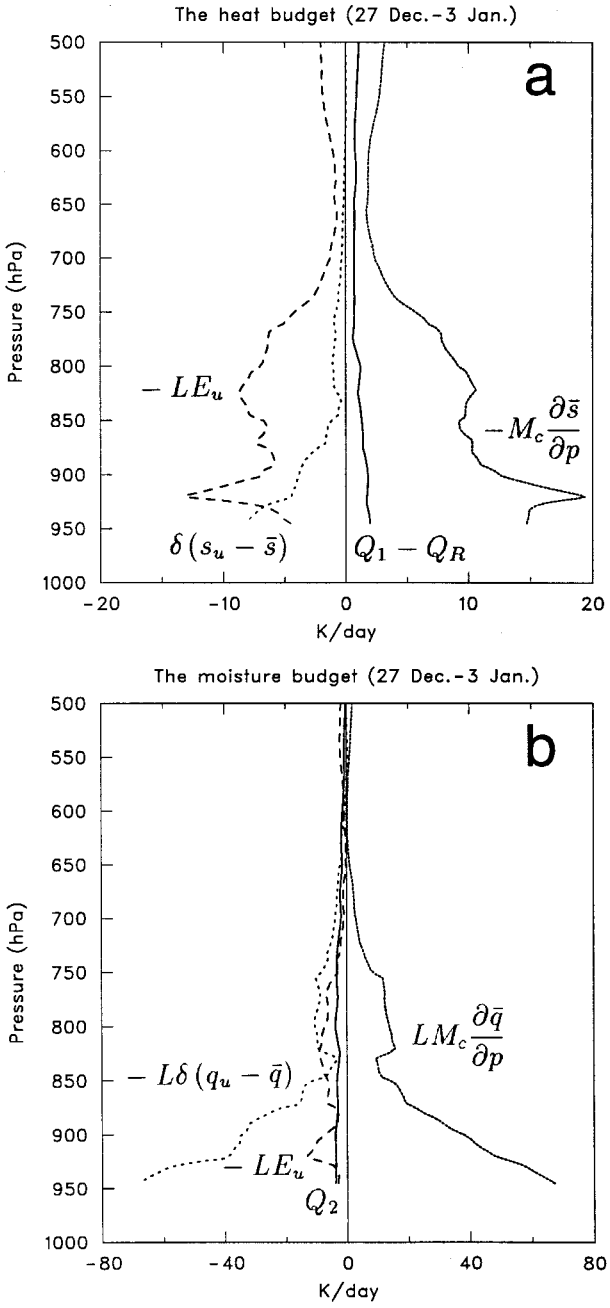

FIG. 12. (a) Heat and (b) moisture balances for the 27 December–3 January westerly wind burst.

As shown, for example, by Nitta (1975), $m_B(\lambda)$ can be obtained from

$$Q_1 - Q_2 - Q_R = \delta(p)(h_D - \bar{h}) - \frac{\partial \bar{h}}{\partial p}\int_0^{\lambda_D(p)} m_B(\lambda)\eta(p, \lambda)\, d\lambda, \quad (6)$$

where h_D is the cloud moist static energy ($c_pT + gz + Lq$) at the detrainment level. In solving (6) it is assumed that the virtual temperature excess at cloud base and cloud top is zero (as in Johnson 1976). IFA-averaged fields at 6-h intervals during the westerly wind bursts are used in the computations.

a. Late December–early January westerly wind burst

Profiles of saturation moist static energy $\bar{h}^*$ and moist static energy at cloud-top detrainment level h_D [from Eq. (15) of Johnson (1976)] for the period 27 Decem-

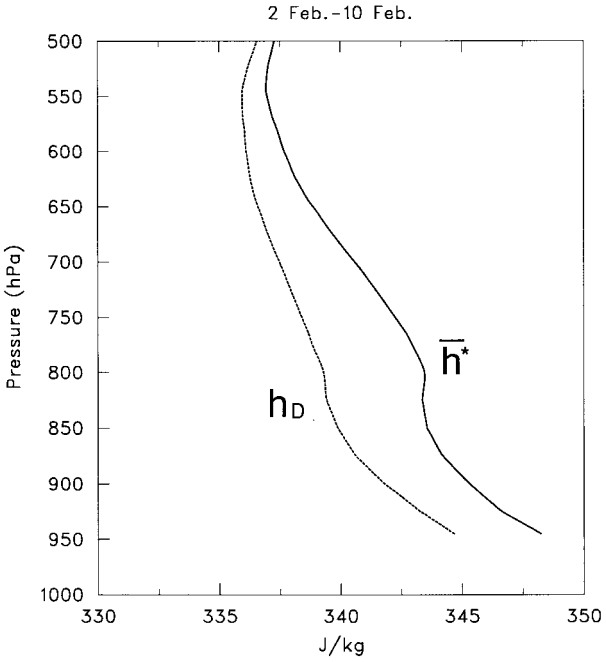

FIG. 13. As in Fig. 9 except for the 2–10 February westerly wind burst.

ber–3 January are shown in Fig. 9. Evidence of a weak trade inversion can be seen in an ~100 hPa layer centered near 800 hPa where h^* increases with height.[3] While this inversion is not nearly as strong as the trade inversion during undisturbed periods in the western Atlantic BOMEX region (Nitta and Esbensen 1974, Fig. 4 upper panel; Nitta 1975, Fig. 4), it does resemble those observed during disturbed periods of the Atlantic trades (Nitta and Esbensen 1974, Fig. 4 lower panel; Nitta 1975, Figs. 10 and 14). While the inversion in Fig. 9 is relatively weak, it is still of sufficient strength to retard the growth of cumulus clouds and lead to a trade-like cumulus population over the warm pool (Schubert et al. 1995; Mapes and Zuidema 1996; Johnson et al. 1996). Compared to other periods of the IOP, the inversion near 800 hPa is particularly strong during the late-December westerly wind burst (Figs. 1a and 7 of Johnson et al. 1996).

During the 27 December–3 January period, average precipitation over most of the IFA was relatively light as a consequence of extreme vertical wind shear, low-to midtropospheric drying and reduced SSTs (Lin and

[3] Averaging of slightly variable inversion heights has smoothed the profile somewhat; however, the stable layer over the warm pool is still considerably weaker than that observed in the Alantic trades (Johnson et al. 1996).

FIG. 14. A photograph taken from the R/V *Vickers* (2.1°S, 156.3°E) in the evening of 6, 7, or 8 February 1993 (courtesy of R. Cifelli). The photograph shows shallow cumulus with tops near 1.5 km (assuming a cloud base of ~0.5 km).

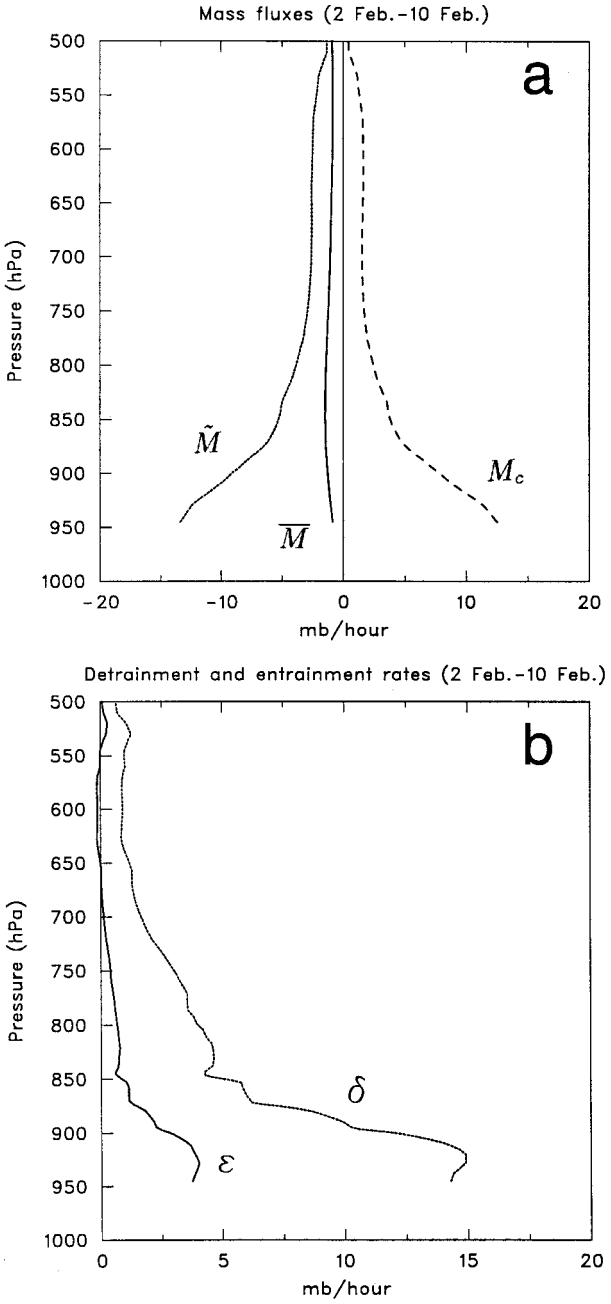

FIG. 15. As in Fig. 11 except for the 2–10 February westerly wind burst.

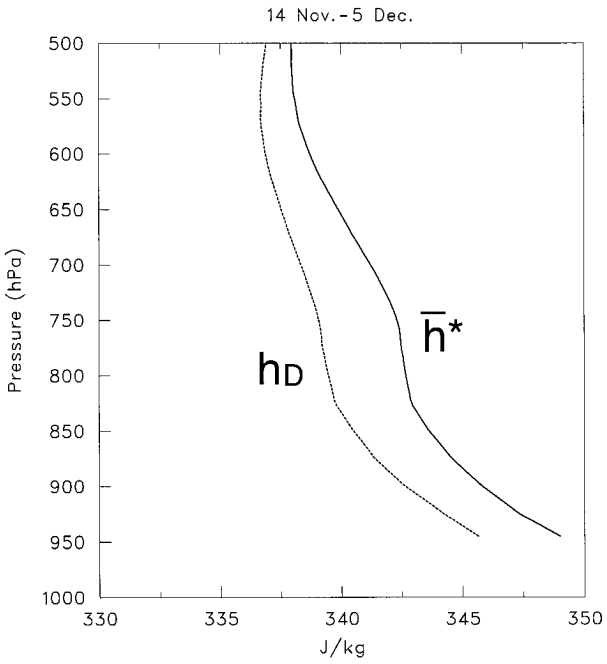

FIG. 16. As in Fig. 9 except for the 14 November–5 December suppressed, light-wind period.

Johnson 1996a): P_0 averaged <6 mm day^{-1} (Fig. 5) although inspection of satellite data indicates that much of the rainfall occurred over the southern part of the IFA. Apart from the abundant mid- and high-level clouds present early in this period (Velden and Young 1994) the predominant cloud type was shallow cumulus, as illustrated in the photograph (Fig. 10) from the R/V *Vickers* at 2.1°S, 156.3°E on 26 December (one day prior to this westerly wind burst period).

Evidence of this shallow cloud field can be seen in the profiles of mass fluxes, entrainment ε, and detrainment δ averaged over the 34% of the 27 December–4 January 6-hourly sounding times for which $P_0 < 3.5$ mm day^{-1} (Fig. 11). Large values of cloud and environmental mass flux, M_c and $\tilde{M}$, can be seen below 900 hPa with the mean mass flux $\overline{M}$ being a small residual. Entrainment and detrainment both peak near cloud base, but there are secondary peaks between 750 and 820 hPa where clouds lose their buoyancy near the trade inversion. This result is clear evidence of an *active tradelike cumulus field during the westerly wind bursts.* These findings are very similar to the BOMEX tradewind results of Nitta (1975) except that the detrainment peak for this westerly wind burst over the western Pacific warm pool extends slightly above the inversion, whereas the Atlantic peaks (at least for two out of the three cases presented by Nitta) are slightly below. This difference may be a consequence of the much-weaker inversion over the warm pool, which allows for greater cloud-top overshooting and some detrainment above the inversion.

The heat and moisture balances (Fig. 12) show cooling and moistening due to evaporation of detrained cloud water ($-LE_u$) near cloud top or between 750 and 850 hPa. Detrainment of heat or $\delta(s_u - \overline{s})$ (which is a cooling effect in this case since the virtual temperature excess at cloud base is assumed to be zero) is important in the lowest 50–100 hPa of the cloud layer. These detrainment cooling effects are offset by subsidence warming $(-M_c \partial \overline{s}/\partial p)$. Detrainment of water vapor $\delta(q_u - \overline{q})$ is an important moistening effect near cloud base and cloud top. The combined detrainment moistening effects are offset by subsidence drying ($LM_c \partial \overline{q}/$

FIG. 17. A photograph taken from the *Xiangyanghong 5* (2.0°S, 155.8°E) on 21 November 1992 by X. Lin. The photograph shows shallow cumulus with tops near 2–2.5 km (assuming a cloud base of ~0.5 km). Ocean waves in foreground are from ship.

∂p). These heat and moisture balance results are qualitatively similar to those of Nitta (1975) and Nitta and So (1980) for other shallow cumulus regimes. They most closely resemble Nitta's (1975) BOMEX Periods 2 and 3 when the trades were disrupted by an upper-level trough and an organized cloud cluster, respectively (Nitta 1975, Figs. 13 and 19). During these BOMEX disturbed periods, the trade inversion weakened considerably and some deep convection coexisted with trade cumulus, much as was observed during the COARE westerly wind bursts. This mixture of convective regimes may account for $\bar{M} \approx 0$ during this westerly burst period.

b. Early February westerly wind burst

Mean profiles of $\bar{h}^*$ and h_D for the period 2–10 February (67% of the 6-hourly sounding times) are shown in Fig. 13. Evidence of a trade inversion again appears near 800 hPa, but it is slightly weaker than during the first westerly wind burst (cf. Fig. 9). Another photograph from the R/V *Vickers* during the February period illustrates the prevalence of shallow clouds (Fig. 14). Many of these clouds have the appearance of subinversion (Esbensen 1978) or forced (Stull 1985) cumuli that are vertical extensions of boundary layer turbulence. The mass fluxes, entrainment and detrainment profiles (Fig. 15) are similar to those before with a secondary peak in detrainment between 800 and 850 hPa. The detrainment peak is a bit weaker than during the December–January period owing to the slightly weaker inversion. The heat and moisture balances are qualitatively similar to those shown in Fig. 12, so they will not be presented.

c. Late November/early December suppressed, light-wind period

Mean profiles of $\bar{h}^*$ and h_D for the 14 November–5 December (representing 50% of the 6-hourly sounding times) are shown in Fig. 16. This period was generally characterized by light winds and mostly clear skies. A trade stable layer can again be seen, but it is weaker and about 50 hPa higher than during the westerly wind bursts. Also, below the trade stable layer, the moist static energy at cloud top h_D during the light-wind period is about 1 J kg^{-1} higher than during the westerly wind bursts. Correspondingly, the SST during the light-wind period was also about 1 K higher (Lin and Johnson 1996b; Weller and Anderson 1996). A photograph from *Xiangyanghong 5* during this period (Fig. 17) shows towering cumulus extending to near the top of the trade stable layer (~2.5 km), with some evidence of spreading and detrainment near that level (e.g., as in Malkus 1954). The deeper clouds resemble the inversion-penetrating cumulus of Esbensen (1978) or active cumulus of Stull (1985). The mass fluxes and entrainment and detrainment profiles (Fig. 18) are similar to those for the west-

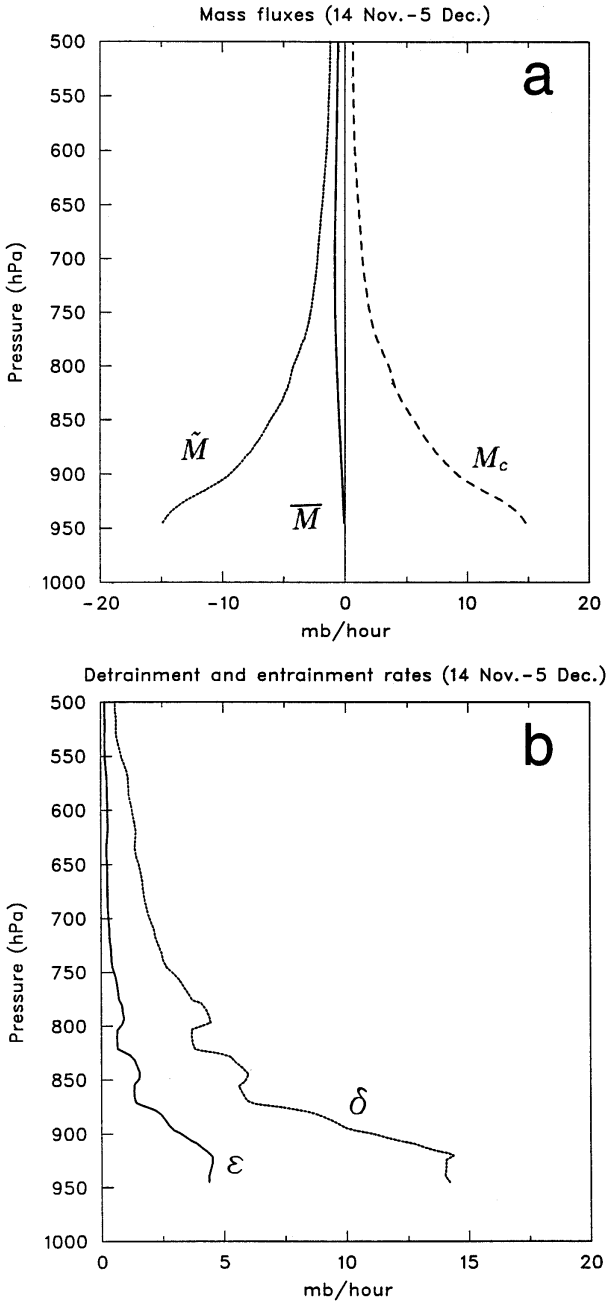

FIG. 18. As in Fig. 11 except for 14 November–5 December suppressed, light-wind period.

erly burst periods except that the upper detrainment peak is about 20–30 hPa higher than those for the westerly wind burst cases.

d. Discussion

The above results for both the westerly wind burst and suppressed, light-wind periods indicate that trade-like cumulus regimes are prevalent over the equatorial western Pacific during the nonprecipitating phases of the 30–60 day intraseasonal oscillation. These findings are consistent with other recent studies (Schubert et al. 1995; Mapes and Zuidema 1996; Johnson et al. 1996), which show trade-stable layers to be commonplace over the equatorial Pacific. Distinctions exist, however, between the shallow cumuli during light- and strong-wind periods. When winds are strong, there is considerable moistening (negative Q_2) in the lower part of the cloud layer (Figs. 7a and 7b) where detrainment rates are large (particularly during the December–January burst, Fig. 11), presumably in association with many subinversion or forced cumuli that represent upward extensions of boundary layer turbulence (Esbensen 1978; Stull 1985). When winds are light, the cumulus are active and extend to a somewhat higher level (as does the trade stable layer), aided by the slightly higher SSTs during light-wind conditions. The profile of Q_2 during this period shows a peak in the upper part of the cloud layer (Fig. 7c), much like the Atlantic trade wind regime (Nitta and Esbensen 1974).

5. Summary and conclusions

Sounding data taken during TOGA COARE reveal a wide range of spatial and temporal variability in the atmospheric heat and moisture budgets. During periods of deep convection, the vertical profiles of the apparent heat source Q_1 and apparent moisture sink Q_2 over the Intensive Flux Array closely resemble those diagnosed elsewhere in the western Pacific ITCZ regions (e.g., Nitta 1972; Yanai et al. 1973). These profiles are also similar to the 4-month mean Q_1 and Q_2 profiles for the extensive area represented by the Outer Sounding Array (OSA). However, over the smaller IFA area and on shorter timescales (weeks) the mean Q_1 and Q_2 profiles are strikingly different. In particular, during westerly wind bursts and suppressed, light-wind periods, these profiles are characterized by negative Q_1 and Q_2 throughout much of the lowest 2 km. These profiles resemble those observed in tradewind cumulus regime of the western Atlantic (Nitta and Esbensen 1974; Nitta 1975) and the convective mixed layer over the East China Sea during cold air outbreaks (Nitta and So 1980).

However, there are noticeable differences in the shallow cumulus between the strong- and light-wind periods. When winds are strong, there is greater moistening (negative Q_2) near cloud base in association with subinversion (Esbensen 1978) or forced (Stull 1985) type cumuli that are, in part, a manifestation of overshooting boundary layer eddies. When winds are light, the cumulus are slightly deeper [''inversion penetrating'' after Esbensen (1978) or ''active'' after Stull (1985)] and the moistening peaks in the upper part of the cloud layer (similar to the Atlantic trades; Nitta and Esbensen 1974). Higher SST (by 1 K) and weaker wind shear during the latter period likely contribute to the more active cumuli at that time.

The cloud spectral diagnostic method of Ogura and

Cho (1973) and Nitta (1975) has been applied to the study of the shallow cumulus fields during two westerly wind burst periods, 27 December–3 January and 2–10 February, and a suppressed, light-wind period, 14 November–5 December. Computed profiles of mass fluxes, entrainment, detrainment, and heat and moisture balances all resemble those for the western Atlantic trades (particularly the somewhat disturbed trades; Nitta 1975) during these periods. This finding leads to the conclusion that the *equatorial western Pacific warm pool boundary layer develops trade-wind-like characteristics with abundant shallow cumulus during both westerly wind bursts and suppressed, light-wind periods and these episodic ''tradelike'' regimes are prominent enough to impact the seasonal (IOP-mean) distributions of boundary-layer heating and moistening.* Also, it is concluded that generalization of seasonal-mean heating and moistening profiles from one region to another over the warm pool (Fig. 2), even if seasonal-average precipitation is approximately the same, is not recommended (see also Lin and Johnson 1996b). The shallow cumulus play an important role in moistening the lower troposphere—either counterbalancing (in some cases) the strong drying effects of ''dry intrusions'' (Mapes and Zuidema 1996; Numaguti et al. 1995; Yoneyama and Fujitani 1995) or preparing the atmosphere for further deep convection following westerly wind bursts. Clearly, their effects will need to be included (parameterized or explicitly represented) in any realistic simulation or treatment of boundary layer processes associated with intraseasonal oscillations and westerly wind bursts over the western Pacific warm pool.

Acknowledgments. Thanks are extended to Dr. Jeffrey Kiehl for use of the CCM2 radiation code and to Drs. Robert Cifelli and Thomas Rickenbach for use of the photographs in Figs. 10 and 14. Paul Ciesielski, Rick Taft, and Jim Bresch have also helped significantly in a number of ways throughout the study. The comments of Peggy LeMone, Alan Betts, and an anonymous reviewer led to significant improvements in the manuscript. This research has been supported by the National Oceanic and Atmospheric Administration under Grant NA37RJ0202.

REFERENCES

Arakawa, A., and W. H. Schubert, 1974: Interaction of a cumulus cloud ensemble with the large-scale environment, Part I. *J. Atmos. Sci.,* **31,** 674–701.

Augstein, E., H. Riehl, F. Ostapoff, and V. Wagner, 1973: Mass and energy transports in an undisturbed Atlantic trade-wind flow. *Mon. Wea. Rev.*, **101,** 101–111.

Barnes, G. M., J. C. Fankhauser, and W. D. Browning, 1996: Evolution of the vertical mass flux and diagnosed net lateral mixing in isolated convective clouds. *Mon. Wea. Rev.*, **124,** 2764–2784.

Betts, A. K., 1975: Parametric interpretation of trade-wind cumulus budget studies. *J. Atmos. Sci.,* **32,** 1934–1945.

——, and B. A. Albrecht, 1987: Conserved variable analysis of the convective boundary layer thermodynamic structure over the tropical oceans. *J. Atmos. Sci.,* **44,** 83–99.

Brümmer, B., 1978: Mass and energy budgets of a 1-km high atmospheric box over the GATE C-scale triangle during undisturbed and disturbed weather conditions. *J. Atmos. Sci.,* **35,** 997–1011.

Chen, S. S., R. A. Houze Jr., and B. E. Mapes, 1996: Multiscale variability of deep convection in relation to large-scale circulation during TOGA COARE. *J. Atmos. Sci.,* **53,** 1380–1409.

Ciesielski, P. E., L. M. Hartten, and R. H. Johnson, 1997: Impacts of merging profiler and rawinsonde winds on TOGA COARE analyses. *J. Atmos. Oceanic Technol.,* in press.

Esbensen, S., 1975: An analysis of subcloud-layer heat and moisture budgets in the western Atlantic trades. *J. Atmos. Sci.,* **32,** 1921–1933.

——, 1978: Bulk thermodynamic effects and properties of small tropical cumuli. *J. Atmos. Sci.,* **35,** 826–837,

Fairall, C. W., E. F. Bradley, D. P. Rogers, J. B. Edson, and G. S. Young, 1996: Bulk paramaterization of air–sea fluxes for TOGA COARE. *J. Geophys. Res.,* **101**(C2), 3747–3764.

Gutzler, D. S., G. N. Kiladis, G. A. Meehl, K. M. Weickmann, and M. Wheeler, 1994: The global climate of December 1992–February 1993. Part II: Large-scale variability across the tropical western Pacific during TOGA COARE. *J. Climate,* **7,** 1606–1622.

Hartmann, D. L., H. H. Hendon, and R. A. Houze Jr., 1984: Some implications of the mesoscale circulations in tropical cloud clusters for large-scale dynamics and climate. *J. Atmos. Sci.,* **41,** 113–121.

Johnson, R. H., 1976: The role of convective-scale precipitation downdrafts in cumulus and synoptic-scale interactions. *J. Atmos. Sci.,* **33,** 1890–1910.

——, 1984: Partitioning tropical heat and moisture budgets into cumulus and meso-scale components: Implication for cumulus parameterization. *Mon. Wea. Rev.,* **112,** 1590–1601.

——, P. E. Ciesielski, and K. A. Hart, 1996: Tropical inversions near the 0°C level. *J. Atmos. Sci.,* **53,** 1838–1855.

Kiehl, J. T., J. J. Hack, and B. P. Briegleb, 1994: The simulated earth radiation budget of the National Center for Atmospheric Research community climate model CCM2 and comparisons with the Earth Radiation Budget Experiment (ERBE). *J. Geophys. Res.,* **99,** 20 815–20 827.

Kiladis, G. N., H. von Storch, and H. van Loon, 1989: Origin of the South Pacific convergence zone. *J. Climate,* **2,** 1185–1195.

——, G. A. Meehl, and K. M. Weickmann, 1994: Large-scale circulation associated with westerly wind bursts and deep convection over the western equatorial Pacific. *J. Geophys. Res.,* **99**(D9), 18 527–18 544.

Legates, D. R., and C. J. Wilmott, 1990: Mean seasonal and spatial variability in gauge-corrected, global precipitation. *Int. J. Climatol.,* **10,** 111–127.

LeMone, M. A., and W. T. Pennell, 1976: The relationship of trade wind cumulus distribution to subcloud layer fluxes and structure. *Mon. Wea. Rev.,* **104,** 524–539.

Lin, X., and R. H. Johnson, 1996a: Kinematic and thermodynamic characteristics of the flow over the western Pacific warm pool during TOGA COARE. *J. Atmos. Sci.,* **53,** 695–715.

——, and ——, 1996b: Heating, moistening and rainfall over the western Pacific warm pool during TOGA COARE. *J. Atmos. Sci.,* **53,** 3367–3383.

Luo, H., and M. Yanai, 1984: The large-scale circulation and heat sources over the Tibetan Plateau and surrounding areas during the early summer of 1979. Part II: Heat and moisture budgets. *Mon. Wea. Rev.,* **112,** 966–989.

Madden, R. A., and P. R. Julian, 1971: Detection of a 40–50 oscillation in the zonal wind in the tropical Pacific. *J. Atmos. Sci.,* **28,** 702–708.

Malkus, J. S., 1954: Some results of a trade-cumulus cloud investigation. *J. Meteor.,* **11,** 220–237.

——, 1955: On the formation and structure of downdrafts in cumulus clouds. *J. Meteor.*, **12,** 350–354.
——, and H. Riehl, 1964: Cloud structure and distribution over the tropical Pacific Ocean. *Tellus,* **16,** 275–287.
Mapes, B. E., and P. Zuidema, 1996: Radiative–dynamical consequences of dry tongues in the tropical atmosphere. *J. Atmos. Sci.,* **53,** 620–638.
Masuda, K., 1984: Diabatic heating during the FGGE: A preliminary report. *J. Meteor. Soc. Japan,* **62,** 702–708.
Nakazawa, T., 1988: Tropical super cluster within intraseasonal variations over the western Pacific. *J. Meteor. Soc. Japan,* **66,** 823–839.
Nicholls, S., and M. A. LeMone, 1980: The fair weather boundary layer in GATE: The relationship of subcloud fluxes and structure to the distribution and enhancement of cumulus clouds. *J. Atmos. Sci.,* **37,** 2051–2067.
Nitta, T., 1972: Energy budget of wave disturbances over the Marshall Islands during the years of 1956 and 1958. *J. Meteor. Soc. Japan,* **50,** 71–84.
——, 1975: Observational determination of cloud mass flux distributions. *J. Atmos. Sci.,* **32,** 73–91.
——, and S. Esbensen, 1974: Heat and moisture budget analyses using BOMEX data. *Mon. Wea. Rev.,* **102,** 17–28.
——, and S. S. So, 1980: Structure and heat, moisture and momentum budgets of a convective mixed layer during AMTEX'75. *J. Meteor. Soc. Japan,* **58,** 378–393.
Numaguti, A., R. Oki, K. Nakamura, K. Tsuboki, N. Misawa, T. Asai, and Y.-M. Kodama 1995: 4–5-day-period variations and low-level dry air observed in the equatorial western Pacific during the TOGA COARE IOP. *J. Meteor. Soc. Japan,* **73,** 267–290.
Ogura, Y., and H.-R. Cho, 1973: Diagnostic determination of cumulus populations from large-scale variables. *J. Atmos. Sci.,* **30,** 1276–1286.
Parsons, D., W. Dabberdt, H. Cole, T. Hock, C. Martin, A.-L. Barrett, E. Miller, M. Spowart, M. Howard, W. Ecklund, D. Carter, K. Gage, and J. Wilson, 1994: The Integrated Sounding System: Description and preliminary observations from TOGA COARE. *Bull. Amer. Meteor. Soc.,* **75,** 553–567.
Pennell, W. T., and M. A. LeMone, 1974: An experimental study of turbulence structure in the fair weather trade wind boundary layer. *J. Atmos. Sci.,* **31,** 1308–1323.
Perry, K. D., and P. V. Hobbs, 1996: Influences of isolated cumulus clouds on the humidity of their surroundings. *J. Atmos. Sci.,* **53,** 159–174.
Reed, R. J., and E. E. Recker, 1971: Structure and properties of synoptic-scale wave disturbances in the equatorial western Pacific. *J. Atmos. Sci.,* **28,** 1117–1133.
Reynolds, R. W., and T. M. Smith, 1995: A high-resolution global sea surface temperature climatology. *J. Climate,* **8,** 1571–1583.
Rickenbach, T. M., 1996: Convection in TOGA COARE: Horizontal scale, morphology, and rainfall production. Ph.D. dissertation, Colorado State University, Fort Collins, 155 pp.
Riehl, H., T. C. Yeh, J. S. Malkus, and N. E. LaSeur, 1951: The northeast trade of the Pacific Ocean. *Quart. J. Roy. Meteor. Soc.,* **77,** 598–626.
Schubert, W. H., P. E. Ciesielski, C. Lu, and R. H. Johnson, 1995: Dynamical adjustment of the trade wind inversion layer. *J. Atmos. Sci.,* **52,** 2941–2952.
Spencer, R. W., 1993: Global oceanic precipitation from the MSU during 1979–91 and comparisons to other climatologies. *J. Climate,* **6,** 1301–1326.
Squires, P., 1958: Penetrative downdrafts in cumuli. *Tellus,* **10,** 381–389.
Stull, R. B., 1985: A fair-weather cumulus cloud classification scheme for mixed-layer studies. *J. Climate Appl. Meteor.,* **24,** 49–56.
Sui, C. H., and K.-M. Lau, 1989: Origin of low-frequency (intraseasonal) oscillations in the tropical atmosphere. Part II. Structure and propagation of mobile wave-CISK modes and their modification by lower boundary forcings. *J. Atmos. Sci.,* **46,** 37–56.
Taylor, R. C., 1973: An atlas of Pacific islands rainfall. Hawaii Institute of Geophysics Rep. HIG-73-9, 7 pp. [Available from Dept. of Meteorology, University of Hawaii at Manoa, 2525 Correa Road, Honolulu, HI 96822.]
Telford, J. W., and P. B. Wagner, 1980: The dynamical and liquid water structure of small cumulus as determined from its environment. *Pure Appl. Geophys.*, **118,** 935–952.
Velden, C. S., and J. A. Young, 1994: Satellite observations during TOGA COARE: Large-scale descriptive overview. *Mon. Wea. Rev.*, **122,** 2426–2441.
Webster, P. J., and R. Lukas, 1992: TOGA COARE: The Coupled Ocean–Atmosphere Response Experiment. *Bull. Amer. Meteor. Soc.,* **73,** 1377–1416.
Wei, M.-Y., D. R. Johnson, and R. D. Townsend, 1983: Seasonal distributions of diabatic heating during the First GARP Global Experiment. *Tellus,* **35A,** 241–255.
Weller, R. A., and S. P. Anderson, 1996: Surface meteorology and air–sea fluxes in the western equatorial Pacific during the TOGA Coupled Ocean–Atmosphere Response Experiment. *J. Climate,* **9,** 1959–1990.
Williams, A. G., H. Kraus, and J. M. Hacker, 1996: Transport processes in the tropical warm pool boundary layer. Part I: Spectral composition of fluxes. *J. Atmos. Sci.,* **53,** 1187–1202.
Yanai, M., S. Esbensen, and J. H. Chu, 1973: Determination of bulk properties of tropical cloud clusters from large-scale heat and moisture budgets. *J. Atmos. Sci.,* **30,** 611–627.
Yoneyama, K., and T. Fujitani, 1995: The behavior of dry westerly air associated with convection observed during TOGA COARE R/V *Natsushima* cruise. *J. Meteor. Soc. Japan,* **73,** 291–304.